Journal for Multiscale Computational Engineering, 11 (6): 505–525 (2013)

ADAPTIVE ATOMISTIC-CONTINUUM MODELING OF DEFECT INTERACTION WITH THE DEBDM

Philip Moseley,[1] Jay Oswald,[2,*] & Ted Belytschko[1]

[1]*Department of Mechanical Engineering, Northwestern University, Evanston, Illinois, USA*

[2]*School for Engineering of Matter, Transport and Energy, Arizona State University, Phoenix, Arizona, USA*

[*]Address all correspondence to Jay Oswald, E-mail: j-oswald@asu.edu

New procedures for modeling interactions among dislocations and nanosized cracks within the dynamically evolving bridging domain method (DEBDM) have been developed. The DEBDM is an efficient concurrent atomistic-to-continuum approach based on the bridging domain method, where the atomic domain dynamically adapts to encompass evolving defects. New algorithms for identifying and coarse graining dislocation-induced slip planes have been added to the method, which previously focused on fracture. Additional improvements include continuously varying BDM energy-weighting functions, which allow the fine-graining and coarse-graining transitions to occur smoothly over multiple timesteps, reducing the potential for nonphysical or unstable behavior. Several examples of interacting dislocations and nanocracks are presented to demonstrate the flexibility and efficiency of the method.

KEY WORDS: *adaptivity, concurrent multiscale, bridging domain method, extended finite element method, fracture, crack propagation*

1. INTRODUCTION

The influence of the interactions of atomic-scale defects on the macroscopic properties of materials is becoming increasingly important for accurate predictions of material behavior, particularly in extreme conditions and for the design a materials tailored for specific applications. One difficulty in quantifying defect interactions is the vast range of spatial and temporal scales that defects such as dislocations, micro-nanocracks, and voids reside in. Not only should numerical models span the spatial and temporal dimensions of the defects being studied, they also must provide suitable boundary and initial conditions so that simulation domain boundaries do not act as artificial barriers to defect propagation. A successful example is the coupled atomistic and discrete dislocation model, where dislocations can propagate from an atomic domain to a continuum one (Qu et al., 2005; Shilkrot et al., 2004).

Multiscale modeling techniques attempt to address these difficulties by resolving fine-scale and coarse-scale information with separate models and linking them either by hierarchical or concurrent coupling schemes. In hierarchical coupling, fine-scale solutions are averaged to act as a surrogate for the constitutive relationship at the coarse scale. In concurrent coupling, multiple models are solved simultaneously in different subdomains of a problem geometry. The objective of this paper is to present recent improvements on an adaptive concurrent modeling scheme where dislocations and cracks are represented at both the continuum and atomistic scales.

Due to the large body of existing literature focused on concurrently coupling atomic and continuum models, a brief review of some recent efforts provides context for our approach. One of the earliest methods for coupling molecular dynamics with finite element calculations was devised by Mullins and Dokainish (1982), where a finite element model was used to provide a boundary condition for a crack in α-iron. This concept was extended to three levels: continuum, molecular dynamics, and tight-binding calculations by Abraham et al. (1998) and Broughton et al. (1999) to study brittle fracture in silicon.

1543–1649/13/$35.00

More recent methods for coupling the atomic and continuum domains include the Arlequin method (Bauman et al., 2008; Ben Dhia, 1998) and the bridging domain method (Belytschko and Xiao, 2003; Xiao and Belytschko, 2004), both of which utilize an overlapping coupling region and Lagrange multiplier constraints to enforce compatibility. Miller and Tadmor (2009) describe these and other coupling methods in detail in their review article.

An important aspect of the coupling method is the ability to exactly reproduce a linear displacement field and therefore satisfy a patch test. Modifications to the Arlequin method have been developed to eliminate spurious ghost forces and satisfy the patch test Chamoin et al. (2010). Another similar approach in Fish et al. (2007) is based on a blending of the continuum stress and atomic forces, where the patch test was demonstrated for a multibody interaction embedded atom method (EAM) potential.

A second issue that arises in dynamic simulations is the spurious reflection of high-frequency waves at the coupling interface. This occurs because of the mismatch in impedance between the atomic and continuum regions, due to the discretization of the continuum. One method that has been largely successful in suppressing spurious reflections is the quasicontinuum (QC) method (Tadmor et al., 1996). In the QC method, the atomic and continuum scales are blended by refining the finite element (FE) mesh to atomic length scales at the boundary of the atomic domain (Miller and Tadmor, 2002; Shenoy et al., 1998). Although the smooth transition of the mesh toward the atomic scale greatly reduces spurious wave reflections, it comes at the cost of extensive mesh refinement. The bridging domain method (BDM) has also been shown to suppress spurious wave reflections when the constraint equations for ensuring compatibility are diagonalized, (Xu and Belytschko, 2008).

The application of the extended finite element method (XFEM) to atomic-to-continuum coupling Gracie and Belytschko (2008, 2011) and modeling of atomic defects (Oswald et al., 2009) has expanded the capability of continuum methods to incorporate features at the atomic level into the continuum description and reduce the requirement for mesh refinement at the atomic-to-continuum interface. The XFEM, developed originally to model crack growth without remeshing (Belytschko and Black, 1999; Moës et al., 1999), has been successfully applied to many other types of problems where interfaces and discontinuities are present, including dislocations (Gracie et al., 2008), shear bands (Areias and Belytschko, 2006), two-phase fluids (Chessa and Belytschko, 2003), and composites (Belytschko et al., 2003).

An adaptive concurrent multiscale formulation is proposed where enrichments to the finite element basis functions allow discontinuities resulting from fracture and slip to be represented within a continuum model. In this formulation, regions characterized by evolving defects, such as dislocation cores and crack tips, are modeled by molecular dynamics, and the remainder of the domain is simulated by a continuum that admits discontinuities via the XFEM. Constraints are imposed through Lagrange multipliers that enforce compatibility between the atomic and continuum levels. In Section 2, the discrete equations of motion for the continuum and atomic regions are derived from Lagrangian mechanics. In Section 3, we describe the coarse and fine-graining algorithms that enable adaptivity in the BDM. Section 4 gives a smoothed formulation for time-varying weight functions that reduces the potential for unphysical behavior generated by the model adaptation. Example problems involving the interaction of multiple cracks and dislocation follow in Section 5, and concluding remarks are given in Section 6.

2. MODEL AND GOVERNING EQUATIONS

The notation for the continuum and atomistic domains are Ω^C and Ω^A, respectively. Capitalized Latin subscripts (I, J, K) denote indices of continuum nodes. Lowercase Greek subscripts (α, β, γ) denote indices of atoms. Boldface indicates a vector or tensor quantity, where vectors will usually be lowercase, and tensors uppercase. The exception will be uppercase vectors referring to reference (undeformed) coordinates such as $\mathbf{X}$, versus lowercase current coordinates $\mathbf{x}$. Unless otherwise noted, summation is implied over repeated subscript indices.

2.1 Extended Finite Element Description

The continuum displacement field is approximated with an enriched finite element basis, as described in Belytschko et al. (2009). This allows continuously varying fields to be described with a standard finite element approximation,

and discontinuities such as cracks and dislocations to be described through the extended finite element method. The displacement field is written as

$$\mathbf{u}(\mathbf{X}) = N_I(\mathbf{X})\mathbf{u}_I + \Psi_J(\mathbf{X})\boldsymbol{\psi}_J, \tag{2.1}$$

where N represents standard finite element shape functions that exist on all nodes, Ψ is enriched shape functions that exist only on a subset of the nodes, and $\mathbf{u}$ and $\boldsymbol{\psi}$ are the nodal degrees of freedom corresponding to the standard and enriched shape functions, respectively. The discontinuities for cracks and dislocations are introduced to the displacement field through the shifted Heaviside function $\Psi(\mathbf{X})$ developed in Ventura et al. (2009). The Heaviside function is suitable for well-defined cracks in crystalline solids.

By constructing a vector $\mathbf{d}$ to hold all continuum degrees of freedom and a vector of all shape functions $\boldsymbol{\Phi}$, the continuum displacement approximation (2.1) can be written more compactly as

$$\mathbf{u}(\mathbf{X}) = \begin{bmatrix} N_I(\mathbf{X}) & \Psi_J(\mathbf{X}) \end{bmatrix} \begin{bmatrix} \mathbf{u}_I \\ \boldsymbol{\psi}_J \end{bmatrix} = \boldsymbol{\Phi}(\mathbf{X}) \cdot \mathbf{d} \tag{2.2}$$

In finite elements which are not enriched, $\boldsymbol{\Psi}$ and $\boldsymbol{\psi}$ equal zero and (2.2) reduces to the standard finite element formulation.

2.2 Governing Equations

The Lagrangian of a general atomistic–continuum system with coupling is written as the sum of the atomistic, coupling, and continuum contributions,

$$\mathcal{L}^A = \sum_\alpha w(\mathbf{X}_\alpha)\frac{m_\alpha}{2}\mathbf{v}_\alpha \cdot \mathbf{v}_\alpha - \overline{W}^A(\mathbf{x}_\alpha, \mathbf{X}_\alpha) \tag{2.3}$$

$$\mathcal{L}^B = \sum_{\beta \in \mathcal{S}^B} \boldsymbol{\lambda}_\beta \left[\mathbf{u}(\mathbf{X}_\beta) - \mathbf{u}_\beta\right] \tag{2.4}$$

$$\mathcal{L}^C = \int_{\Omega_0^C} \left[(1 - w(\mathbf{X}))\left(\frac{\rho_0(\mathbf{X})}{2}\dot{\mathbf{u}}(\mathbf{X}) \cdot \dot{\mathbf{u}}(\mathbf{X}) - W^C(\mathbf{C}(\mathbf{X}))\right)\right] d\Omega_0^C \tag{2.5}$$

where $\mathcal{L}^A$ and $\mathcal{L}^B$ are respectively the atomistic and coupling (bridging) Lagrangian equations, and $\mathcal{L}^C$ is the continuum Lagrangian density. W^C is the continuum strain energy density. The atomic mass, current position, and velocity of atom α are given by m_α^A, $\mathbf{x}_\alpha$, and $\mathbf{v}_\alpha$. The function $w(\mathbf{X})$ is a weighting or blending function that allows for a continuous transition between continuum and atomistic domains, ranging from zero (fully continuum) and one (fully atomistic), as shown in Fig. 1. Variables that include the blending weight are written with an overline, e.g., $\overline{\bullet}$. The set of Lagrange multipliers $\boldsymbol{\lambda}_\beta$ couple the scales by enforcing the atomic displacements $\mathbf{u}_\beta$ to equal the continuum displacements $\mathbf{u}(\mathbf{X}_\beta)$ for the set of atoms in the bridging domain, $\mathcal{S}^B$.

The weighted atomic energy $\overline{W}^A$ is a global quantity that is a function of both the atomic potentials and the blending function w. The empirical potentials ϕ that estimate the energy of a configuration of atoms are generally made up of pairwise and multibody terms. Thus, $\overline{W}^A$ can be written

$$\overline{W}^A(\mathbf{x}_\alpha, \mathbf{X}_\alpha) = \sum_{\beta \in \mathcal{N}_\alpha} w(\mathbf{X}_\alpha, \mathbf{X}_\beta)\phi_2(r_{\alpha\beta}) + \sum_{\beta \in \mathcal{N}_\alpha}\sum_{\gamma > \beta} w(\mathbf{X}_\alpha, \mathbf{X}_\beta, \mathbf{X}_\gamma)\phi_3(\hat{\mathbf{r}}) + \ldots \tag{2.6}$$

where $\mathcal{N}_\alpha$ is the set of atoms interacting with atom α, and bond weights are evaluated at the bond midpoints. Ghost atoms are used at the edge of the BDM domain to maintain consistent forces. In composite lattices the secondary lattice atoms should remain free of BDM constraints to allow internal relaxation, as described in Xu et al. (2010). However, the weighting scheme developed in that paper is limited to nearest-neighbor interactions, so we maintain the

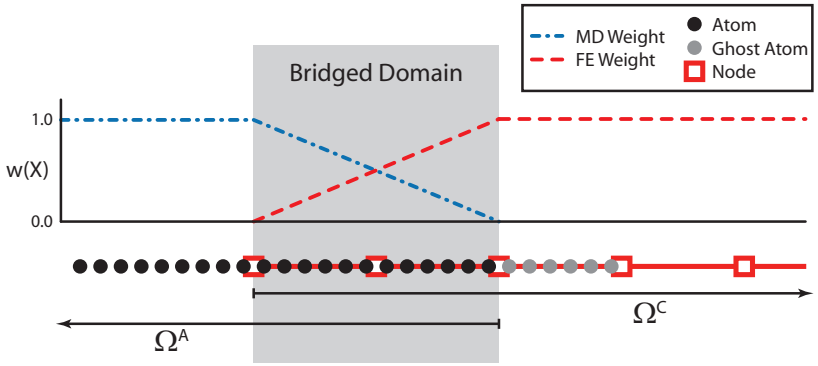

FIG. 1: Bridging domain method, with ghost atoms

conventional averaging weighting scheme described above and accomplish the same equilibrium effect by applying forces asymmetrically, i.e., between atoms existing on the primary and secondary sublattices, the force applied is

$$\bar{\mathbf{f}}_\alpha = \begin{cases} w(\mathbf{X}_\alpha, \mathbf{X}_\beta)\mathbf{f}_\alpha & \alpha \in \text{ primary lattice} \\ \mathbf{f}_\alpha & \alpha \in \text{ secondary lattice} \end{cases} \tag{2.7}$$

The equations of motion are derived from the Euler-Lagrange equations. For the coupled atomistic-to-continuum system, the Euler-Lagrange equations are

$$\frac{d}{dt}\frac{\partial \mathcal{L}^A}{\partial \dot{\mathbf{u}}_\alpha} - \frac{\partial \mathcal{L}^A}{\partial \mathbf{u}_\alpha} - \frac{\partial \mathcal{L}^B}{\partial \mathbf{u}_\beta} = 0 \tag{2.8}$$

$$\frac{\partial \mathcal{L}^B}{\partial \boldsymbol{\lambda}_\beta} = 0 \tag{2.9}$$

$$\frac{d}{dt}\frac{\partial \mathcal{L}^C}{\partial \dot{\mathbf{u}}(\mathbf{X})} + \frac{\partial}{\partial \mathbf{X}} \cdot \frac{\partial \mathcal{L}^C}{\partial \mathbf{F}(\mathbf{X})} + \frac{\partial \mathcal{L}^B}{\partial \mathbf{u}(\mathbf{X})} = 0 \tag{2.10}$$

After solving, the equations are

$$w(\mathbf{X}_\alpha) m_\alpha \ddot{\mathbf{u}}_\alpha + \frac{\partial \overline{W}^A}{\partial \mathbf{u}_\alpha} + s_{\alpha\beta}\boldsymbol{\lambda}_\beta = 0 \tag{2.11}$$

$$\mathbf{u}(\mathbf{X}_\beta) - \mathbf{u}_\beta = 0 \tag{2.12}$$

$$(1 - w(\mathbf{X}))\left(\rho_0(\mathbf{X})\ddot{\mathbf{u}}(\mathbf{X}) + \frac{\partial}{\partial \mathbf{X}} \cdot \frac{\partial W^C}{\partial \mathbf{F}(\mathbf{X})}\right) + \sum_I s_I \Phi_I(\mathbf{X}_\beta)\boldsymbol{\lambda}_\beta = 0 \tag{2.13}$$

where $s_{\alpha\beta} = \delta_{\alpha\beta}$ if β is in a coupling domain, and vanishes otherwise, and s_I is 1 if node I is in the coupling domain and 0 otherwise.

Note that in Section 4 this formulation is modified in order to introduce transitions between scales which occur smoothly over time during adaptivity.

2.3 Discrete Equations

The discrete equations are as in Xiao and Belytschko (2004), where the atomic and nodal masses, respectively, are calculated using

$$\overline{m}_\alpha = w(\mathbf{X}_\alpha) m_\alpha, \qquad \overline{m}_{IJ} = \int_{\Omega_0^C} (1 - w)\rho_0 \Phi_I \Phi_J d\Omega_0^C \tag{2.14}$$

Internal forces for the atomic and continuum domains are calculated using

$$\overline{\mathbf{f}}_{\alpha}^{\text{int}} = \frac{\partial \overline{W}^{A}}{\partial \mathbf{x}}, \qquad \overline{\mathbf{f}}_{I}^{\text{int}} = \int_{\Omega_0^C} (1-w) \frac{\partial \Phi_I}{\partial \mathbf{X}} \cdot \mathbf{S} \cdot \mathbf{F}^T d\Omega_0^C \tag{2.15}$$

Additional forces on the atoms and nodes come from the coupling constraints,

$$\mathbf{f}_{\alpha}^{\text{bdm}} = s_{\alpha\beta} \boldsymbol{\lambda}_{\beta}, \qquad \mathbf{f}_{I}^{\text{bdm}} = -s_I \Phi_I(\mathbf{X}_{\alpha}) \boldsymbol{\lambda}_{\alpha} \tag{2.16}$$

where the Lagrange multipliers $\boldsymbol{\lambda}$ come from solving

$$-\frac{2}{\Delta t} \mathbf{g}_{\alpha}^{*} = A_{\alpha\beta} \boldsymbol{\lambda}_{\beta} \tag{2.17}$$

with $A_{\alpha\beta}$ and $\mathbf{g}_{\alpha}^{*}$ defined as

$$A_{\alpha\beta} = \sum_{I \in \varphi} \frac{\Phi_I(\mathbf{X}_{\alpha}) \Phi_I(\mathbf{X}_{\beta})}{\overline{m}_I} + \frac{\delta_{\alpha\beta}}{\overline{m}_{\alpha}} \tag{2.18}$$

$$\mathbf{g}_{\alpha}^{*} = \mathbf{v}_{\alpha}^{*n+1} - \Phi_I(\mathbf{X}_{\alpha}) \dot{\mathbf{d}}_{I}^{*n+1} \tag{2.19}$$

where φ refers to all nodes whose shape functions support includes $\mathbf{X}$, and $\delta_{\alpha\beta}$ is the Kronecker delta.

External forces for the atomic and continuum domains are calculated using

$$\begin{aligned} \overline{\mathbf{f}}_{\alpha}^{\text{ext}} &= w(\mathbf{X}_{\alpha}) \mathbf{f}_{\alpha} \\ \overline{\mathbf{f}}_{I}^{\text{ext}} &= \int_{\Omega_0^C} (1-w) \rho_0 \Phi_I \mathbf{b} d\Omega_0^C + \int_{\Gamma_0^t} (1-w) \Phi_I \bar{\mathbf{t}} d\Gamma_0^t \end{aligned} \tag{2.20}$$

using the standard notation for boundary conditions.

The discrete equations are integrated using a velocity Verlet explicit time integration scheme. The Lagrange multipliers act as forces on the coupled atoms and coupled nodes such that the constraint remains satisfied at the following time step. In order to solve for these unknown constraint forces, a predictor/corrector approach is employed, where the constraint at the following time step is evaluated with trial velocities, and the Lagrange multipliers needed to force the constraint to vanish are solved for at each time step [for the full algorithm see Moseley et al. (2012)].

Note that it is common to diagonalize the A matrix from (2.18) using the row-sum technique,

$$A_{\alpha} = \sum_{\beta} A_{\alpha\beta} \tag{2.21}$$

which is more computationally efficient but dissipates energy. However, Xu and Belytschko (2008) have show the diagonalized form to be more effective in suppressing spurious wave reflections at coupling interfaces.

3. DEBDM ADAPTIVITY

3.1 Domain Decomposition

The model consists of a finite element mesh which covers the entire simulated domain Ω. Atomic domains Ω^A overlay portions of the mesh and the remainder is the continuum domain Ω^C. The atomic domains are defined in terms of the mesh elements ("subdomains") they occupy and are algorithmically divided into three layers, as show in Fig. 2. From innermost to outermost, the layers are as follows:

i. Defects layer, Ω_d^A – The defects layer consists of the atomistic subdomains containing inhomogeneous behavior, such as broken interatomic bonds or strain localization. These are portions of the atomic domain in which the displacement field cannot be accurately approximated by FEM/XFEM.

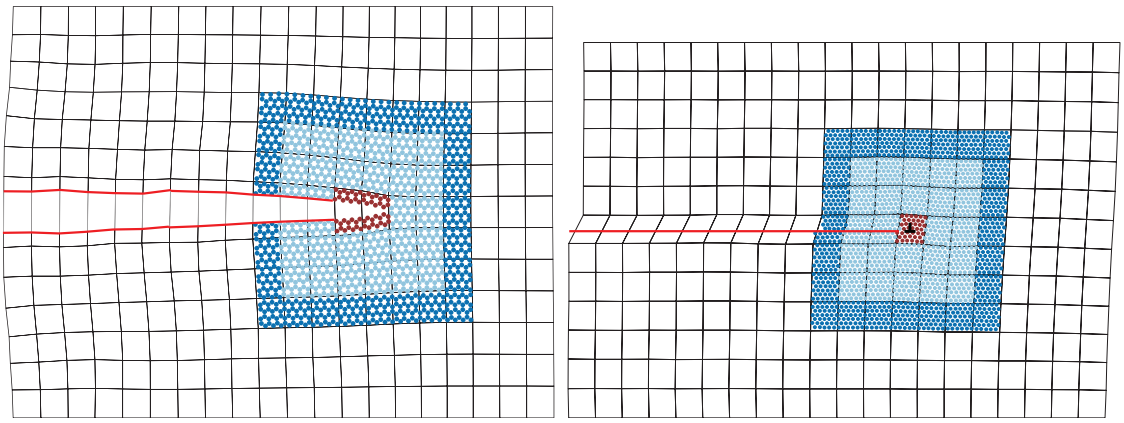

(1) A crack in graphene (2) A dislocation in a hexagonal lattice

FIG. 2: Atomic decomposition: coupling (blue), buffer (light blue), and defect (red) layers

ii. Buffer layer, Ω_b^A – The buffer layer surrounds the defects layer. This region acts to separate the behavior in Ω_d^A from the BDM constraints in the coupling layer.

iii. Coupling (BDM) layer, Ω_c^A – The coupling layer is the outermost layer of atomic subdomains, where BDM coupling occurs.

The layer decompositions are a bookkeeping scheme to simplify the adaptation process. As fine-scale behavior occurs or subsides, subdomains are automatically added or removed from Ω_d^A by the fine-graining and coarse-graining algorithms. Because the buffer and coupling layers are formed around Ω_d^A, this set determines the size and shape of the fine-scale domain. The depth of the buffer layer should be chosen based on the radius of atomic interaction and the speed of defect propagation, such that a defect in the defects layer is not constricted by the BDM constraints. Similarly, the depth of the coupling layer should be adjusted to ensure a smooth transition between scales with no direct interaction between fully MD and ghost atoms. In a mesh with very irregularly sized elements, an adjusted algorithm based on distance from a defect, instead of layers of elements, may be a more efficient means of decomposition.

3.2 Fine-Graining Procedure

Fine-graining transitions elements from the coarse scale (finite element) to the fine scale (molecular dynamics), expanding the atomic region for modeling new fine-scale behavior. The fine-graining procedure (visualized in Fig. 3) consists of three steps:

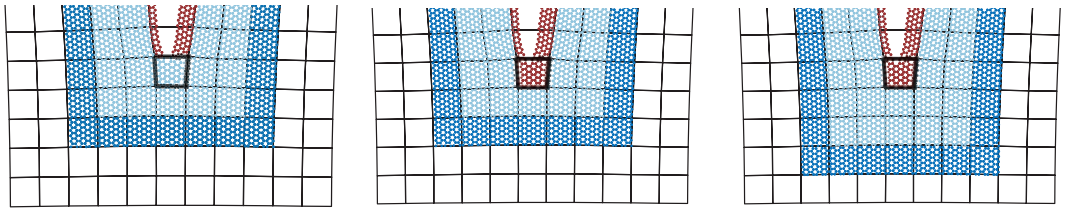

(1) Identification (2) Reclassification (3) Transitioning

FIG. 3: Fine-graining procedure, showing coupling (blue), buffer (light blue), and defect (red) layers with new Ω_d^A element identified with a black ring

i. Identify subdomains in Ω_b^A which contain fine-scale behavior.

ii. Reclassify identified subdomains as Ω_d^A.

iii. Transition the affected subdomains in Ω_b^A and Ω_c^A.

In step 3.2, the buffer layer is checked for behavior indicative of defects. Defects are identified by the existence of any broken interatomic bonds, or by distorted atomic displacement fields which cannot conform to a continuum. In order to check for the latter, nodal displacements are approximated using the atomic data by a best-fit solution to

$$\mathbf{d} = \left(\hat{\mathbf{\Phi}}^T \cdot \hat{\mathbf{\Phi}}\right)^{-1} \left(\hat{\mathbf{\Phi}}^T \cdot \hat{\mathbf{u}}\right) \tag{3.1}$$

Here $\hat{\mathbf{\Phi}}$ is a matrix of the evaluated finite element and extended finite element shape functions, such that each row corresponds to $\mathbf{\Phi}(\mathbf{X}_\alpha)$ from (2.2). Atom α exists in the set of atoms in the support of the shape functions from the nodes in the element, i.e., the set of atoms existing in the element and its neighbors. Similarly, $\hat{\mathbf{u}}$ is the matrix of atomic displacements for these atoms. A quality of fit for each element $\mathbb{E}$ in Ω_b^A is calculated with the R^2 coefficient of determination,

$$\begin{aligned} R^2_{\mathbb{E}} &= 1 - \frac{\sum_{\beta \in \mathbb{E}} \left(||\mathbf{u}_\beta - \mathbf{u}(\mathbf{X}_\beta)||\right)^2}{\sum_{\beta \in \mathbb{E}} \left(||\mathbf{u}_\beta - \overline{\mathbf{u}_\mathbb{E}}||\right)^2} \\ \overline{\mathbf{u}_\mathbb{E}} &= \frac{1}{n} \sum_{\beta \in \mathbb{E}} \mathbf{u}_\beta \end{aligned} \tag{3.2}$$

for the set of n atoms β in element $\mathbb{E}$. If the continuum field matches the atomic displacements perfectly, $||\mathbf{u}_\beta - \mathbf{u}(\mathbf{X}_\beta)|| \equiv 0$ for all atoms $\beta \in \mathbb{E}$, and the R^2 value for the element equals unity. As the quality of fit degrades, the R^2 value decreases. A poor fit, with an R^2 below a given tolerance e^{fg}, indicates the continuum field is unable to model the atomic subdomain with acceptable accuracy, and the element contains fine-scale behavior such as a defect. Higher (more stringent) values of e^{fg} require the finite elements to more closely match the atoms, resulting in more fine graining and increasing the size of the fine-scale domain.

Step ii occurs when subdomains have been identified in step i, using either the broken-bond criterion or the R^2 error criterion. The identified Ω_b^A subdomains are reclassified to Ω_d^A, and the buffer and coupling layers are rebuilt to maintain their specified widths.

Step iii handles the transitions which occur when step ii enlarges the domain. Three different types of transitions can occur: (1) coupling layer Ω_c^A to buffer layer Ω_b^A, (2) continuum domain Ω^C to coupling layer Ω_c^A, or (3) continuum domain directly to the buffer layer. The subdomains reclassified in step ii require no transitioning, as the buffer layer and the defects layer are both fully atomistic. These layers exist solely for bookkeeping purposes during adaptations.

The first type of transition, from Ω_c^A to Ω_b^A, involves subdomains which are described at both the molecular dynamics (MD) and FE scales. Removing the BDM constraints/weights reverts them to fully atomistic. After the transition these atoms are modeled with the rest of the MD domain.

The other two types of transitions involve finite elements with no corresponding atomic description. To create the atoms, an atomic lattice is created which spans the element in the reference (undeformed) configuration and aligns with the reference configurations of other atomic lattices. The positions, velocities, and accelerations of the new atoms are then interpolated from the current continuum fields,

$$\begin{bmatrix} \mathbf{x}_\alpha & \mathbf{v}_\alpha & \mathbf{a}_\alpha \end{bmatrix} = \mathbf{\Phi}(\mathbf{X}_\alpha) \cdot \begin{bmatrix} \mathbf{d} & \dot{\mathbf{d}} & \ddot{\mathbf{d}} \end{bmatrix} \tag{3.3}$$

The new atoms now have all the requisite data to participate in the Verlet time integration. For composite lattices such as graphene, an additional step relaxes the sublattice internal modes. If the transitioning element is becoming part of the fully atomistic buffer layer, the transition is finished. If the element is transitioning to the BDM coupling region, new BDM coupling constraints are calculated on the atoms and nodes.

3.3 Coarse-Graining Procedure

The coarse-graining algorithm attempts to model fine-scale discontinuities using XFEM. Successful coarse graining reduces the number of atomic degrees of freedom, reducing the computational cost of the simulation. The three-step coarse-graining procedure (visualized in Fig. 4) is similar to the fine-graining procedure:

i. Attempt to approximate Ω_d^A subdomains using FEM/XFEM.

ii. Remove identified subdomains from Ω_d^A.

iii. Transition the affected subdomains in surrounding layers.

In Step i, the coarse-graining procedure searches for subdomains in Ω_d^A which can be approximated by the continuum. Subdomains containing a crack tip or dislocation core are excluded from coarse graining, since a coarse-grained defect can no longer propagate. These are identified by examining neighboring subdomains; if a defect has propagated completely through a subdomain, the neighboring subdomains should also contain a discontinuity. If the defect enters a subdomain and does not exit, the defect is allowed to develop further. The remaining Ω_d^A subdomains typically contain crack faces or dislocation slip planes. Solving an iteratively reweighted linear least-squares fit to the reference-coordinate midpoints of the broken bonds in these subdomains provides a level set for the discontinuity,

$$\boldsymbol{\beta}^{\tau+1} = \text{argmin}_{\boldsymbol{\beta}} \sum_{i=0}^{n} w_i\left(\boldsymbol{\beta}^{\tau}\right) ||\mathbf{y} - \mathbf{X}\boldsymbol{\beta}^{\tau}||^2, \qquad w_i\left(\boldsymbol{\beta}\right) = \frac{1}{|y_i - X_{ij}\beta_j|} \tag{3.4}$$

where $\boldsymbol{\beta}$ are the linear coefficients over a number of iterations τ. This reweighting scheme helps to mitigate the effect of outlying points which often occur during fracture as atoms realign along the free surfaces of the crack faces.

Next, the FEM/XFEM degrees of freedom are computed using (3.1), and an R^2 quality of fit is computed using (3.2). Subdomains containing no broken bonds (or where all broken bonds have reformed) are approximated using only the standard FE description. The algorithm continues if R^2 is above a given tolerance e^{cg} for an element. Using a lower (more forgiving) value for e^{cg} will result in more elements being coarse-grained, at the cost of less accurate approximations included in the coarse scale.

In order to determine if the XFEM enrichments should describe a crack or a dislocation, the XFEM degrees of freedom $\boldsymbol{\psi}$ are examined. In a dislocation the XFEM enrichments provide a jump in displacements along the discontinuity, whereas a crack will additionally experience a jump perpendicular to the discontinuity. Therefore dislocations in XFEM can be identified as when the $\boldsymbol{\psi}$ for the element lie along the same angle as the broken bonds, known as the Burger's vector.

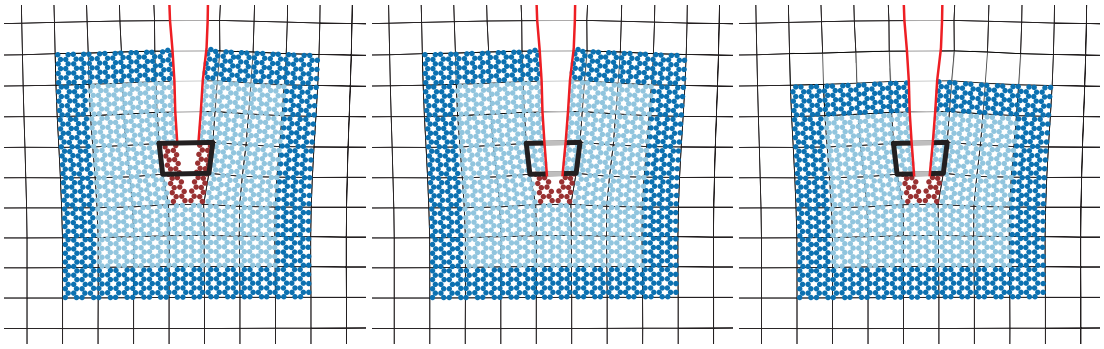

FIG. 4: Coarse-graining procedure, showing coupling (blue), buffer (light blue), and defect (red) layers with new Ω_b^A element identified with a black ring

The process in step i is shown in Fig. 5. The midpoints of broken bonds are shown as X's and are used to compute the XFEM discontinuity for the highlighted element. After initializing the FEM and XFEM degrees of freedom, the discontinuous displacement field matches the atomic displacements extremely well, resulting in an R^2 value close to 1.0. It can be difficult to achieve such good agreement between scales when the fracture behavior is more complex.

Step ii follows by removing the identified subdomains from Ω_d^A, and the buffer and defect layers are modified in order to maintain their specified widths.

Step iii handles the transitions which occur when step ii reduces the size of the fine-scale domain. Three types of transitions can occur: (1) coupling layer Ω_c^A to continuum domain Ω^C, (2) Ω_d^A or Ω_b^A to the coupling layer, or (3) Ω_d^A or Ω_b^A directly to the continuum domain. Typically the subdomains from Ω_d^A become part of Ω_b^A, where they are eligible for fine graining if new behavior occurs. Subdomains which are moved from the defect layer to the buffer layer require no transitioning as they remain fully atomistic.

The first type of transition, from Ω_c^A to Ω^C, involves subdomains which are described at both the MD and FE scales. The atomic lattice in these elements is deleted and the BDM constraints are removed from the nodes; the elements are now fully continuum.

The other two types of transitions involve fully atomistic subdomains for which a FE description is needed. The underlying FEM and XFEM nodes are updated as in (3.1), additionally defining the velocities and accelerations for the nodal degrees of freedom,

$$\begin{bmatrix}\mathbf{d} & \dot{\mathbf{d}} & \ddot{\mathbf{d}}\end{bmatrix} = \left(\hat{\mathbf{\Phi}}^T \cdot \hat{\mathbf{\Phi}}\right)^{-1} \hat{\mathbf{\Phi}}^T \begin{bmatrix}\hat{\mathbf{u}} & \hat{\mathbf{v}} & \hat{\mathbf{a}}\end{bmatrix} \tag{3.5}$$

The transitioned nodes now have all the necessary data to participate in the next cycle of the standard Verlet time integration. Once the continuum description is updated, new BDM coupling constraints are calculated for nodes and atoms as necessary.

While calculating BDM constraints for elements with new XFEM descriptions, some atoms may not conform to the continuum description, as in Fig. 6. This can disturb or separate the atomic lattice, as the coupling constrain's these atoms (shown in red) differently than the MD. These atoms can be identified by calculating their R^2 error,

$$R_\alpha^2 = \frac{\left(||\mathbf{u}_\alpha - \mathbf{u}(\mathbf{X}_\alpha)||\right)^2}{\sum_{\beta\in\mathbb{E}}\left(||\mathbf{u}_\beta - \overline{\mathbf{u}_\mathbb{E}}||\right)^2} \tag{3.6}$$

where $\overline{\mathbf{u}_\beta}$ is defined as in (3.2). Atoms with an R_α^2 greater than a certain tolerance e_α^{cg} can be excluded from BDM constraints to reduce these effects. In this paper, $e_\alpha^{\text{cg}} = 0.0005$.

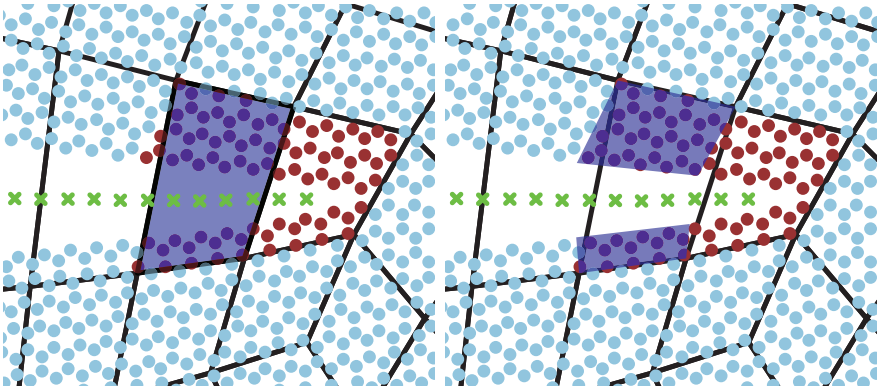

(1) Before XFEM. $R_\mathbb{E}^2 = 0.881399$ (2) After XFEM. $R_\mathbb{E}^2 = 0.999753$

FIG. 5: Computing coarse-grained approximations using broken bonds

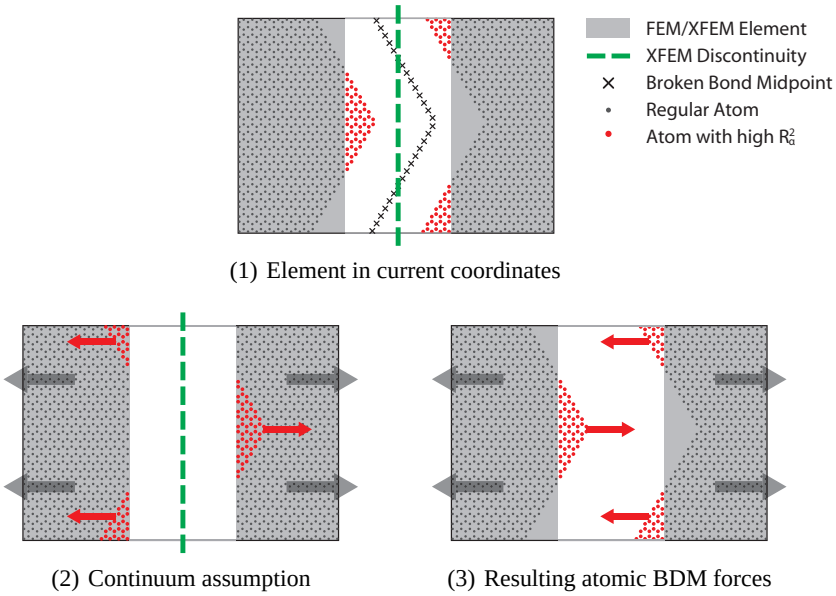

FIG. 6: A difficult element to coarse grain

4. SMOOTHLY TRANSITIONING ADAPTIVITY

The adaptive procedure described in Section 3 works well for most simulations; however, problems can arise during the fine-graining and coarse-graining procedures as subdomains are transitioned between scales. In the method as presented so far and as in Moseley et al. (2012), these transitions occur instantaneously. Because the coarse and fine scales cannot provide precisely the same material approximation, the sudden transition between scales can create a shock on the atoms or nodes as the material adjusts to the new description.

This can be particularly problematic when coarse graining with lower-quality XFEM descriptions, such as the element in Fig. 6. When transitioning elements such as these to fully continuum, approximating nodal data using (3.5) can give unexpected results, even when ignoring certain atoms with e_α^{cg}. Mismatched atomic velocities can cause the nodes to be initialized in incorrect directions or magnitudes. Additionally, transitioning these elements from fully MD to the BDM region and suddenly applying the BDM forces on the atoms can disrupt the lattice, potentially even creating new, nonphysical defects. Similarly, the atomic lattice created while fine graining with (3.3) may not be the optimal configuration, and their sudden addition to the simulation can cause disturbances. This can be an important factor for composite lattices such as graphene, where part of the fine-graining process involves allowing the secondary lattice to relax to relieve internal stresses, and when running simulations at finite temperatures.

In order to reduce these effects, a smooth transitioning scheme has been developed. In this approach, subdomains are gradually transitioned between scales over a range of time steps. The gradual transition avoids any major shocks from differing approximations at different scales. This is accomplished by taking advantage of the BDM weighting functions $w(\mathbf{X})$, which the BDM uses to ensure the transition in space between scales is smooth. By making the weights a function of both time and space $w(\mathbf{X}, t)$, the coarse-graining and fine-graining procedures can adapt smoothly in time.

The time-dependent weighting functions require reevaluation of the Euler-Lagrange Eqs. (2.8), (2.9), and (2.10). Solving these equations with the new weighting functions gives

$$w(\mathbf{X}_\alpha, t) m_\alpha \ddot{\mathbf{u}}_\alpha + \frac{\partial w(\mathbf{X}_\alpha, t)}{\partial t} m_\alpha \dot{\mathbf{u}}_\alpha + \frac{\partial \overline{W}^A}{\partial \mathbf{u}_\alpha} + s_{\alpha\beta} \boldsymbol{\lambda}_\beta = 0 \tag{4.1}$$

$$\mathbf{u}(\mathbf{X}_\beta) - \mathbf{u}_\beta = 0 \tag{4.2}$$

$$[1-w(\mathbf{X},t)]\left(\rho_0(\mathbf{X})\ddot{\mathbf{u}}(\mathbf{X})+\frac{\partial}{\partial\mathbf{X}}\cdot\frac{\partial W^C}{\partial\mathbf{F}(\mathbf{X})}\right)-\frac{\partial w(\mathbf{X},t)}{\partial t}\rho_0(\mathbf{X})\dot{\mathbf{u}}(\mathbf{X})+\sum_I s_I\Phi_I(\mathbf{X}_\beta)\boldsymbol{\lambda}_\beta=0 \tag{4.3}$$

The additional terms here are added to the coupling constraints (2.16) to create an alternate form of the coupling forces,

$$\mathbf{f}_\alpha^{\text{debdm}}=\mathbf{f}_\alpha^{\text{bdm}}-\frac{\partial w(\mathbf{X}_\alpha,t)}{\partial t}m_\alpha\dot{\mathbf{u}}_\alpha,\qquad \mathbf{f}_I^{\text{debdm}}=\mathbf{f}_I^{\text{bdm}}+\sum_{J\in\varphi}\int_{\Omega_0^C}\frac{\partial w(t)}{\partial t}\rho_0\Phi_I\Phi_J d\Omega_0^C\dot{\mathbf{d}}_I \tag{4.4}$$

These are used instead of (2.16) and revert to the standard BDM form when smooth transitions are disabled, e.g., when $(\partial w)/(\partial t)=0$. The modified forces require a new equation for the Lagrange multipliers [replacing (2.17)],

$$-\frac{2}{\Delta t}\mathbf{g}_\alpha^*=A_{\alpha\beta}\boldsymbol{\lambda}_\beta-\mathbf{h}_\alpha^{\text{debdm}}+\sum_{I\in\varphi}\Phi_I(\mathbf{X}_\alpha)\mathbf{h}_I^{\text{debdm}} \tag{4.5}$$

where $\mathbf{h}_\alpha^{\text{debdm}}$ and $\mathbf{h}_I^{\text{debdm}}$ are defined as

$$\mathbf{h}_\alpha^{\text{debdm}}=\frac{\dot{\mathbf{u}}_\alpha}{w(\mathbf{X}_\alpha,t)}\frac{\partial w(\mathbf{X}_\alpha,t)}{\partial t},\qquad \mathbf{h}_I^{\text{debdm}}=\frac{\dot{\mathbf{d}}_I}{\overline{m}_I(t)}\sum_{J\in\varphi}\int_{\Omega_0^C}\frac{\partial w(t)}{\partial t}\rho_0\Phi_I\Phi_J d\Omega_0^C \tag{4.6}$$

Alternately, since the additional force terms in (4.4) do not depend on the Lagrange multipliers $\boldsymbol{\lambda}$, the new force terms can be applied while calculating the accelerations in velocity Verlet integration. In this way the original equation (2.17) for the Lagrange multipliers can still be satisfied.

The procedure is illustrated in Fig. 7 for an element being fine grained. In Fig. 7(1) an initial BDM region is shown in gray, and the element to its right (initially populated with ghost atoms) will be fine grained into the MD domain. The transition begins in Fig. 7(2). Here the MD domain is expanded to include the new element, but the new atoms have a BDM weight of zero such that the element is still fully controlled by the FE degrees of freedom. As the simulation progresses, the weights are gradually readjusted (while maintaining a partition of unity) until they have reached the desired final state [Fig. 7(4)]. At this point the leftmost element of the bridged domain is weighted fully MD, and may be treated as a portion of the standard MD domain and be removed from the BDM calculations. Previously, fine graining involved moving directly from the initial condition in Fig. 7(1) to the final condition in Fig. 7(5). For coarse graining, the process is simply reversed.

In practice, changing the BDM weights every step is computationally expensive, as the masses in (2.14) and constraint matrix A in (2.18) need to be recalculated every time the weights change. Therefore, instead of fully recalculating these values at every time step during a transition, they are precalculated at a certain number of keyframes evenly spaced in time through the transition. The A matrix and masses can then be approximated cheaply and effectively for any time by linearly interpolating between the values at the nearest keyframes.

5. EXAMPLES

5.1 Cracks and Dislocations in Hex Lattice

A two-dimensional sheet of copper atoms in a hexagonal lattice is prestrained 6.15% in the x direction. The sheet is 1200 $\times$ 900 Å, and the left and right sides are fixed in space after applying the prestrain. The atomic potential used is the Morse potential,

$$\phi=D_e\left[\left(1-e^{-\beta(r-r_0)}\right)^2-1\right] \tag{5.1}$$

where D_e = 7.9075 kcal/mol, $\beta=1.3588\,\text{Å}^{-1}$, and r_0 = 2.866 Å for copper, as in Girifalco and Weizer (1959). Additionally, a cutoff radius r_c = 5.5 Å is implemented. The molar mass is 63.546 g/mol. The atomic domain is thermostatted at 1.0°K using the Berendsen thermostat (Berendsen et al., 1984). Rigid body motion can be conveniently calculated for the thermostat by examining nodal velocities approximated from atomic data.

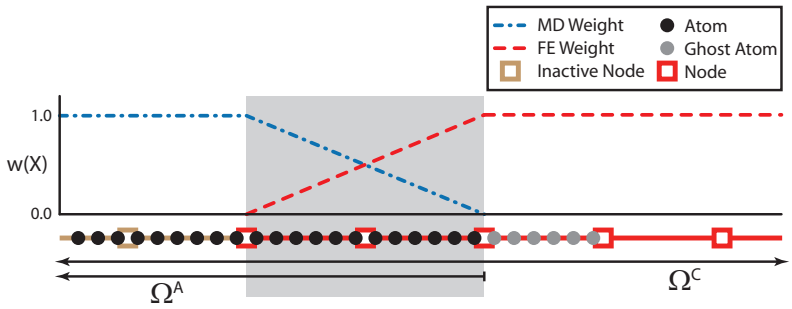

(1) Initial condition

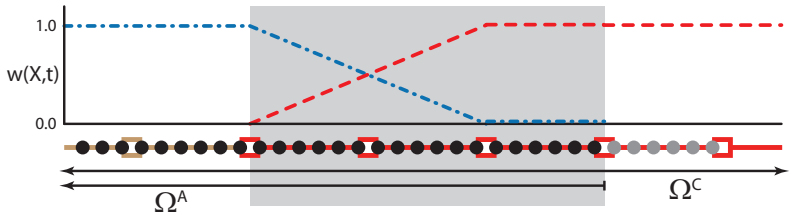

(2) Start of smooth transition, $t = t_{\text{init}}$

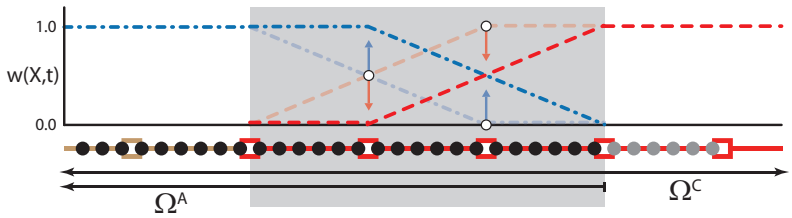

(3) During smooth transition, $t \in (t_{\text{init}}, t_{\text{final}})$

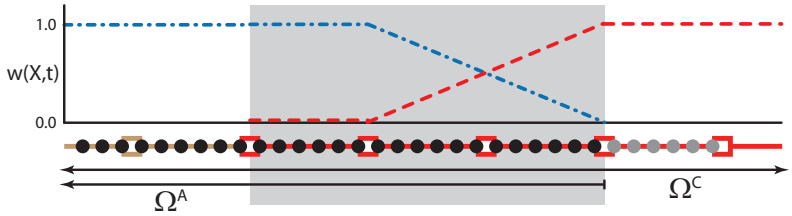

(4) End of smooth transition, $t = t_{\text{final}}$

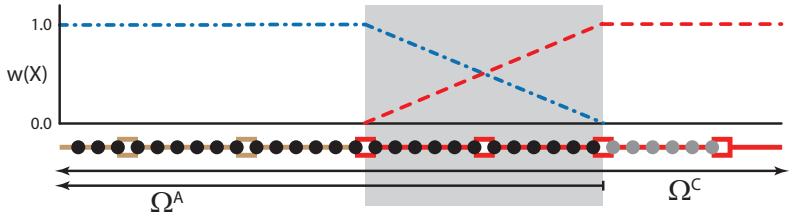

(5) Final condition

FIG. 7: Smoothly transitioning a bridging domain

The finite element mesh is a regular mesh 51 elements by 41 elements, totaling 2091 quadrilaterals, modeled with a constitutive law based on the Cauchy-Born rule. The elements are relatively small; each element is equivalent to a cluster of approximately 80 atoms. The fine resolution of the FE mesh is intended to prevent a single element from having to model multiple dislocations, a current and temporary limitation of our XFEM implementation. The time step for both MD and FE is 2.0 fs, and the problem runs for 30,000 time steps for a total simulation time of 60 ps. Fine graining and coarse graining are attempted every 150 timesteps.

An initial crack is created at the top-middle of the plate by deleting a band of atoms 5.0 Å wide by 25.0 Å tall, and the two finite elements containing the crack are added as the initial subdomains of the core layer of the MD domain. Because the finite elements are relatively small in this problem, the buffer and coupling layers are each two elements deep. The coarse-graining tolerance $e^{\text{cg}} = 0.95$. For this problem the fine-graining occurs solely based on broken bonds; the fine-graining tolerance e^{fg} is not needed.

Figure 8 shows the model at several points during the simulation. XFEM discontinuities are shown as colored lines; green lines represent dislocation slip planes, and red lines represent each surface of a crack. It can be seen that as the crack grows it periodically births dislocations, which propagate away from the crack tip to the edge of the domain, leaving behind an XFEM slip plane. The method is fairly indifferent to dislocation path; it successfully coarse grains slip planes even very close to element corners. As the crack tip speed diminishes, the dislocations occur closer together. New dislocations emanating from the crack tip near times 48.0 and 60.0 ps lie almost directly on top of an existing slip-plane. Currently, our XFEM implementation does not allow us to have multiple XFEM enrichments for a single element, so we are not yet able to apply separate enrichments for both dislocations. Because of this limitation, the algorithm attempts to coarse grain the two neighboring dislocations as a crack, the coarse-graining tolerance is not met, and the elements along the double dislocation remain in MD. This also limits the ability to model branched defects using XFEM, meaning much of the crack is forced to stay in MD due to the large number of dislocations branching from crack surfaces. Future work will alleviate these limitations.

Figures 9 and 10 show additional plots at the end of the simulation, time $t = 60.0$ ps. Figure 9 shows the atomic displacements in the Y direction for both the adaptive solution and the fully MD solution, such that the dislocation slip planes are clearly demarcated by discontinuities in the color gradient. Figure 10 plots the atomic kinetic energy, and the existing dislocation cores can be easily seen as pockets of high energy.

Figure 11 shows the evolution of active degrees of freedom throughout the simulation. The highest number of atoms occurs near the end of the simulation, with close to 50,000. However, the average number of atoms for the simulation is only approximately 23,000. If the precise paths of the crack and dislocations were known beforehand, the minimum number of atoms for this simulation is the same as the number of atoms in a fine-graining-only simulation, approximately 85,000 atoms. Fully atomic simulation requires approximately 160,000 atoms.

The running times of the adaptive solution versus a fully MD solution are shown in Table 1. “Coupling time” includes the time to calculate and apply the Lagrange multipliers each time step, as well as the BDM constraint matrix. “Adapting time” is the time taken to run the fine-graining and coarse-graining algorithms. The majority of the Adapting time is occupied by the coarse-graining algorithm. “IO time” includes time to calculate output data such as energy, as well as the time it takes to write all data (such as nodal/atomic displacements, velocities, accelerations) to disk. In this example, the adaptive solution completes in 58% of the time it takes for the fully MD solution to complete. The speedup will be larger in most simulations which use larger finite elements (such as in an irregular, adapted mesh), or when the simulated domain is larger. For example, consider running the same simulation with the width of the domain doubled. For a fully MD simulation, this would double the number of atoms, doubling the runtime. Using dynamically evolving BDM (DEBDM), the number of atoms remains unchanged; therefore the MD, coupling, and adapting times remain the same. Only the FEM time scales up, plus a small increase in IO time. For such a simulation, the DEBDM approach would run in approximately 38% of the fully MD solution. If the domain width was quadrupled, DEBDM would finish in 28% of the time. Further benefits come with the application of the multi-time-step algorithm in Xiao and Belytschko (2004), which allows the use of different time steps for each scale.

In this example, an additional speedup will come from running the coarse-graining algorithm less often; we have chosen a higher frequency primarily to showcase the coarse-graining algorithms’ capabilities. We anticipate additional benefits to come simply from more efficient code; our code is a research code, and our implementation of the complex algorithms detailed above stands to be improved. The code is C++, running single threaded on an

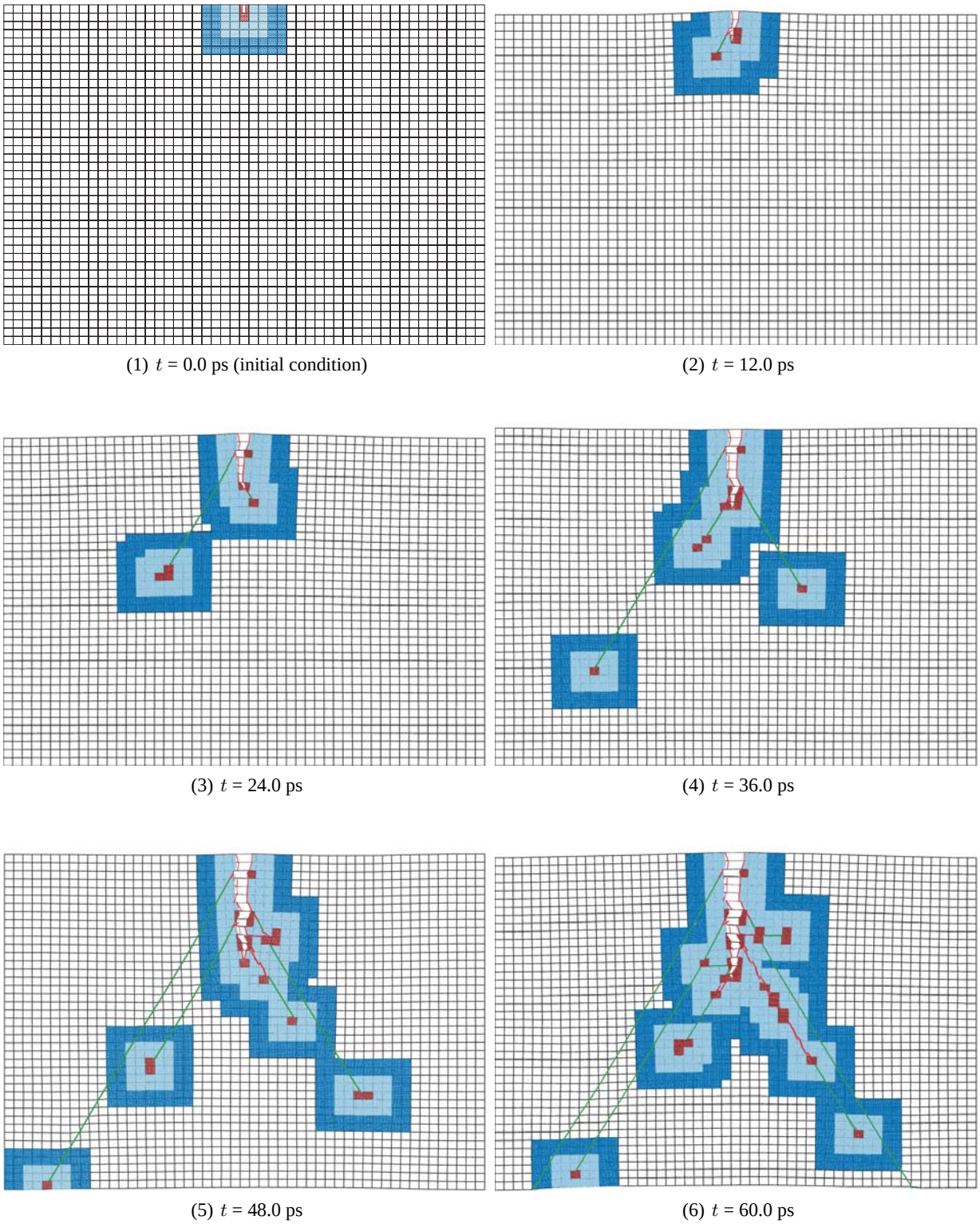

(1) t = 0.0 ps (initial condition)

(2) t = 12.0 ps

(3) t = 24.0 ps

(4) t = 36.0 ps

(5) t = 48.0 ps

(6) t = 60.0 ps

FIG. 8: Example 5.1. Red lines show XFEM crack surfaces, green lines show XFEM dislocation slip planes

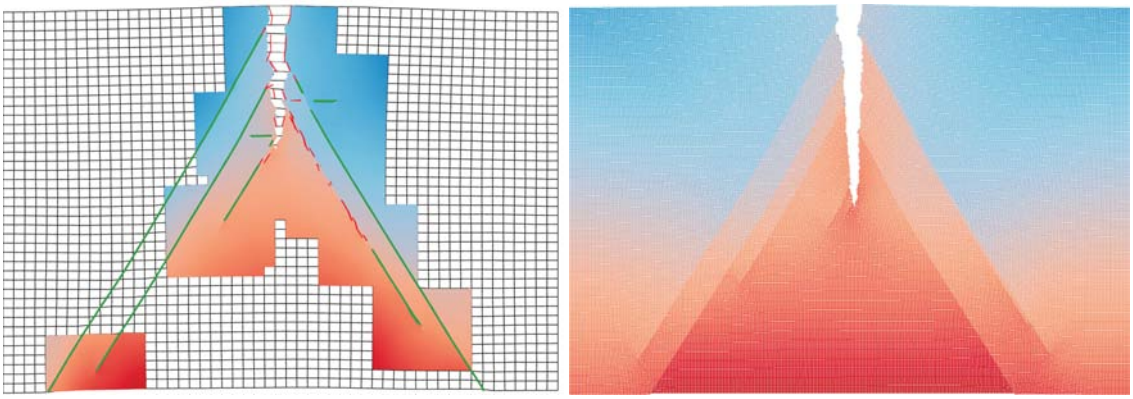

(1) Adaptive solution (2) Fully MD solution

FIG. 9: Atomic displacements in Y for example 5.1

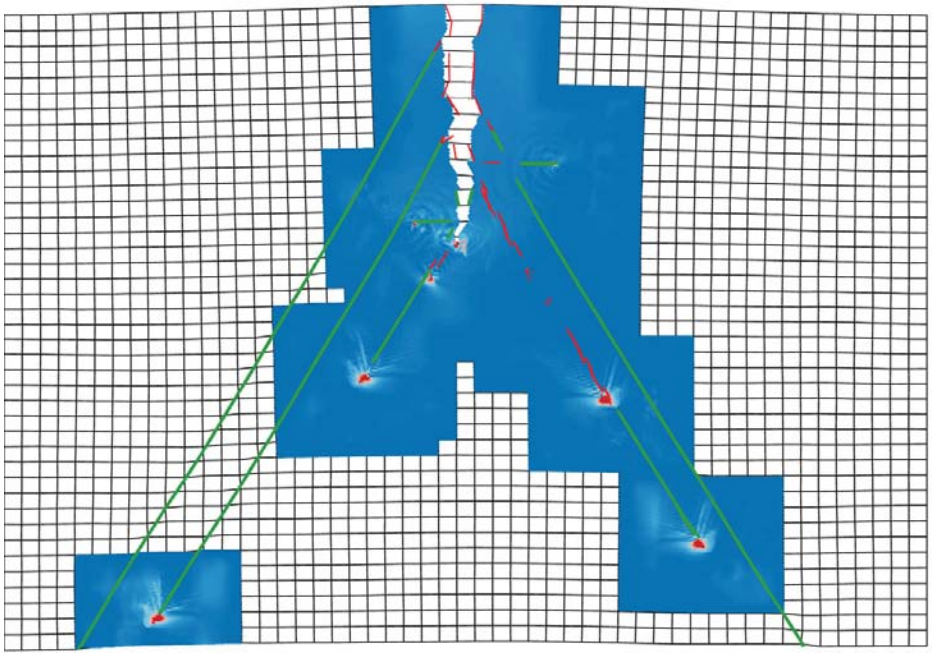

FIG. 10: Kinetic energy between 0.0 and 0.0001 kcal/mol for example 5.1

Intel Core i7-920. Both the fully MD and the adaptive solution were run using the same code base on the same machine.

As can be seen in Fig. 12(1), the Berendsen thermostat maintains a relatively constant temperature in the atomic domain. The energetic input of the thermostat is negligible. However, Fig. 12(2) shows a marked increase in total system energy, ending approximately 10% above the initial levels. The majority of the energy contributions come from the potential energies of the MD and FE. The additional energy appears to correspond primarily with the potential energy associated with dislocation cores and the free surface energy associated with crack surfaces and the edges of the domain.

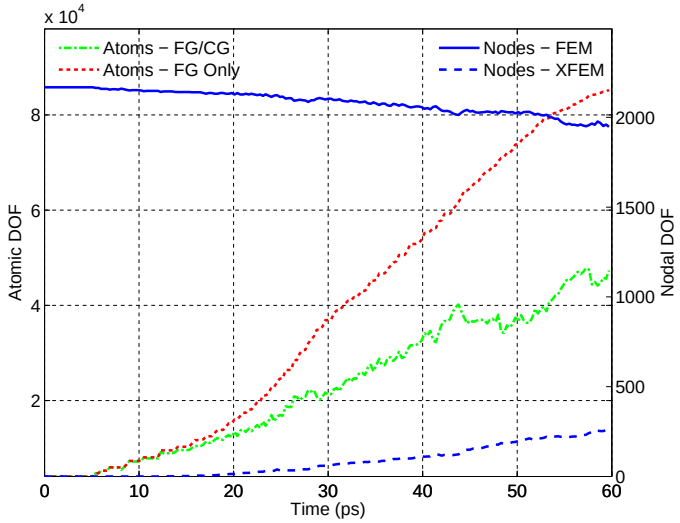

FIG. 11: Degrees of freedom during example 5.1

TABLE 1: Running times of adaptive simulation vs fully MD simulation (hh:mm:ss)

	Adaptive simulation		**Fully MD simulation**	
MD time:	00:19:50	20.76%	02:23:55	87.77%
FEM time:	00:26:27	27.68%		
Coupling time:	00:15:54	16.64%		
Adapting time:	00:30:46	32.20%		
IO time:	00:02:36	02.72%	00:20:03	12.23%
Total time:	01:35:33		02:43:58	

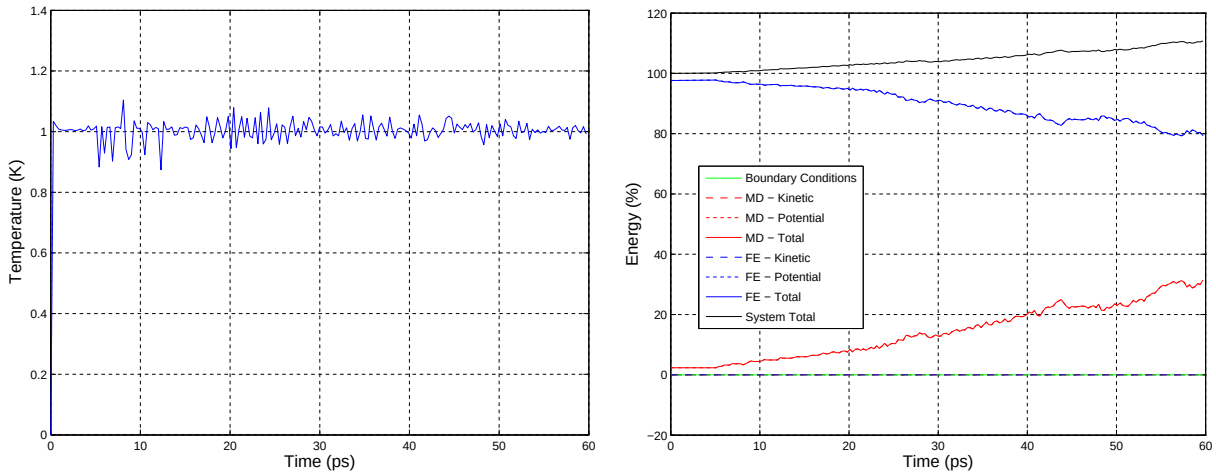

(1) Temperature (2) Energy

FIG. 12: Temperature and energy during example 5.1

5.2 Branching Crack in Graphene

A sheet of single-layer graphene is fractured in the armchair direction. The sheet is 300.0 × 600.0 Å, and is initialized with a prestrain along the y-axis, which varies from 8% to 4%. The top and bottom boundaries are fixed in space. Atoms are deleted to create an initial crack 45 Å long and 5 Å wide in an initial atomistic region on the left side of the plate. The atomic mass for carbon is 12.0107 g/mol, and the atomic potential used is modified Morse from Belytschko et al. (2002):

$$\phi = \phi_{\text{stretch}} + \phi_{\text{angle}}, \;\; \phi_{\text{stretch}} = D_e\left[\left(1 - e^{-\beta(r-r_0)}\right)^2 - 1\right], \;\; \phi_{\text{angle}} = \frac{1}{2}k_\theta\left(\theta - \theta_0\right)^2\left[1 + k_{\text{sextic}}\left(\theta - \theta_0\right)^4\right] \quad (5.2)$$

using the following parameters for graphene from the same source,

$$\begin{array}{lll} r_0 = 1.39\text{Å}, & D_e = 3.764 \text{ eV}, & \beta = 2.625 \text{ Å}^{-1}, \\ \theta_0 = 2.094 \text{ rad}, & k_\theta = 5.617 \text{ eV/rad}^2, & k_{\text{sextic}} = 0.754 \text{ rad}^{-4} \end{array}$$

The buffer and coupling layers have depths of two and one elements, respectively. The adaptivity tolerance for coarse graining is e^{cg}= 0.95, and the fine-graining tolerance is unused in favor of refining solely on broken bonds. The atomic domain is thermostatted at a relatively high temperature of 50.0 K using the Berendsen thermostat, in order to ensure branching occurs.

The finite element mesh is a regular mesh 25 elements by 41 elements, for a total of 1025 quadrilaterals. The constitutive law is based on the Cauchy-Born rule, with an additional step to relax internal lattice modes. Each element is equivalent to a cluster of approximately 100 atoms. The fine resolution allows us to model the changing angles of the branching cracks more closely. The time step is 0.75 fs, and the problem runs 7800 time steps for a total simulation time of 5.85 ps. Fine graining and coarse graining are attempted every 150 time steps, and smooth transitions are enabled which last for 25 time steps.

Figure 13 shows several time steps during the simulation. Note that in several frames the BDM layer is larger than usual due to elements being in midtransition. As the simulation evolves, the crack branches once around t = 1.13 ps, and the top crack branches again around t = 3.38 ps. The outer cracks provide enough stress relief that the third crack begins to close around t = 4.50 ps, and finishes closing up to the branch shortly before the end of the simulation. At the end of the simulation everything has been successfully coarse grained, except for the only remaining crack branch.

The smooth transitions play a key role in this example. Cracks in graphene make sharp turns that can be difficult to coarse grain. When elements containing these angling cracks are coarse grained, assigning nodal velocities and accelerations using 3.5 can result in unstable, nonphysical movement of the FEM/XFEM degrees of freedom. The smooth transitioning dampens out this behavior and can prevent the nodes from oscillating wildly and affecting the simulation. In this problem, this difficulty occurs on the lower branch of the crack, in the two places where it changes direction. When smooth transitioning is not employed, these nodes obtain nonphysical velocities from the atoms and experience high oscillations. The oscillations disrupt the surrounding nodes, causing the atomistic region to explode and the simulation must end. The smooth transitions moderate this. The coarse graining occurs successfully without disrupting the atomic region. It can be seen that the XFEM degrees of freedom in some of the final elements of the lower crack still experience nonphysical behavior. This can be improved further with longer (slower) transitions.

Figure 14(1) shows the evolution of active degrees of freedom throughout the simulation. The average number of atoms present during the simulation is 12,000 atoms. A fully atomic simulation of the model requires approximately 85,000 atoms. The total system energy, shown in Fig. 14(2), also fluctuates over time. The decrease in energy around t = 4.5 ps, which corresponds to a large drop in atomic degrees of freedom (DOF), supports the belief that the atomic potential energy associated with free surfaces is responsible for much of the energy fluctuations. At the end of the simulation, the system energy has risen approximately 5% from the initial conditions.

6. CONCLUSION

Several improvements and updates for the DEBDM method have been presented. The DEBDM method allows propagating and interacting atomic-scale defects to be modeled efficiently by minimal molecular dynamics subdomains. In

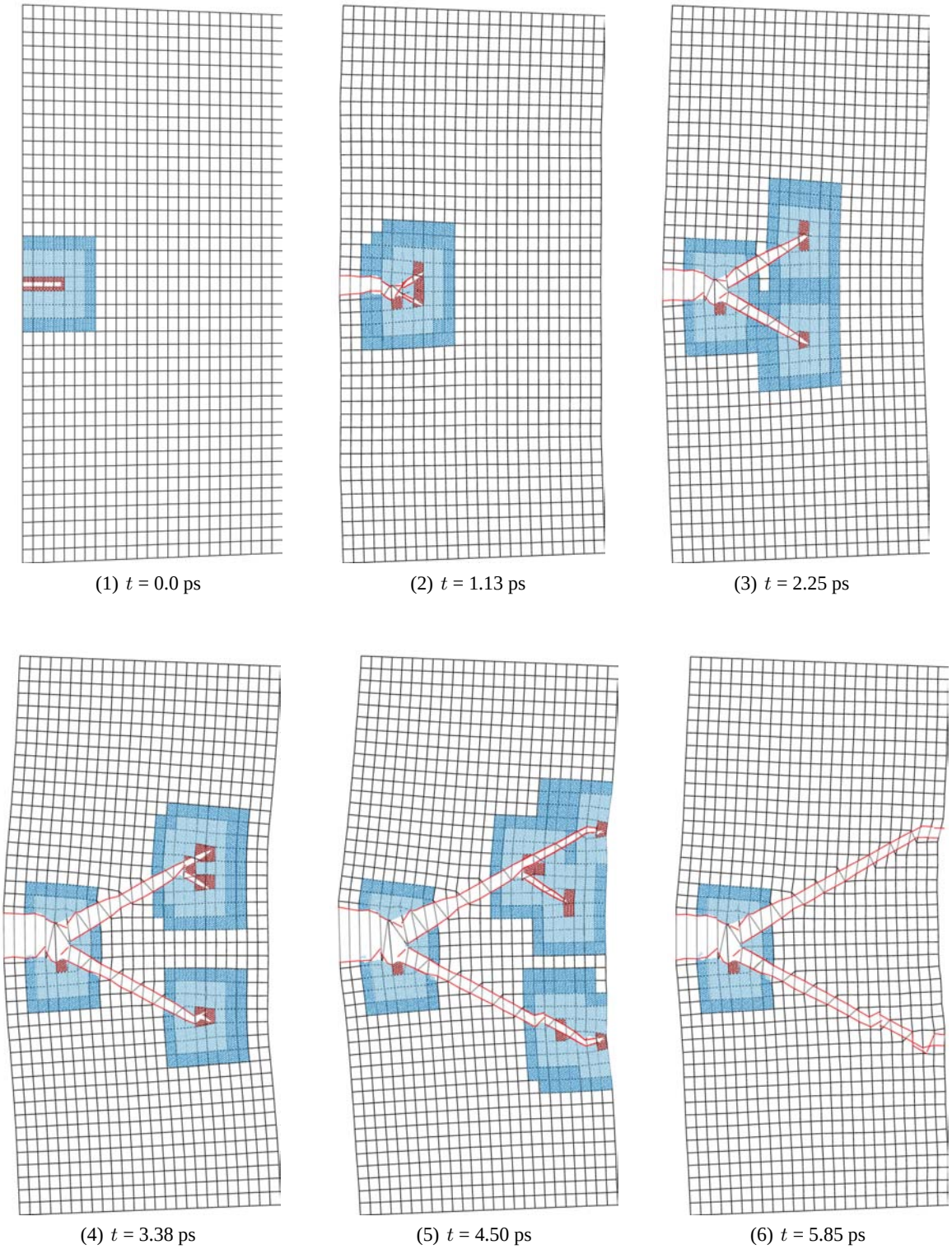

(1) t = 0.0 ps (2) t = 1.13 ps (3) t = 2.25 ps

(4) t = 3.38 ps (5) t = 4.50 ps (6) t = 5.85 ps

FIG. 13: Example 5.2. red lines show XFEM crack surfaces

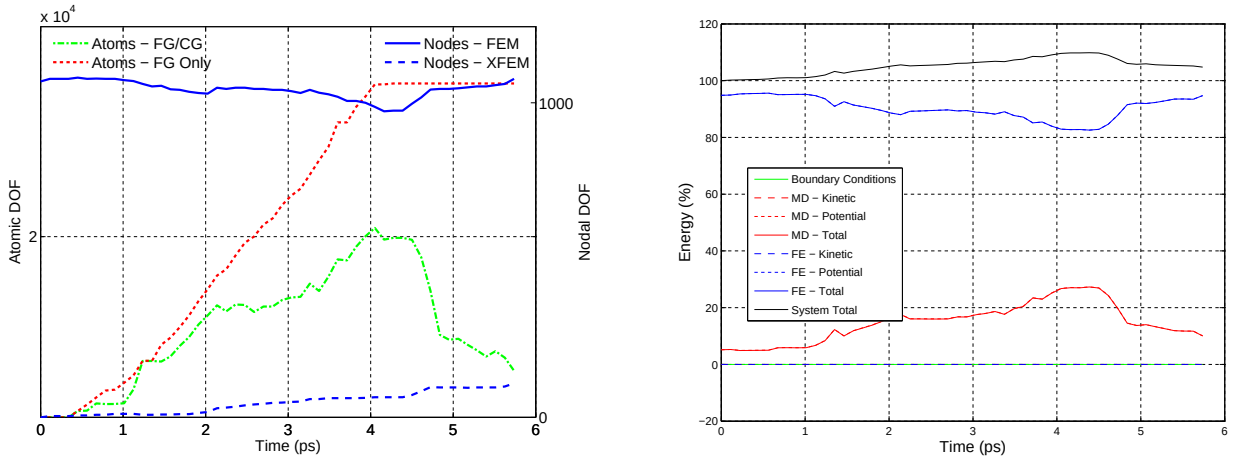

(1) Degrees of freedom (2) Energy

FIG. 14: Energy and degrees of freedom during example 5.2

this paper, the flexibility and robustness of the method is shown by adding support for dislocations as well as cracks. Additional research develops the concept of smooth transitions between scales during adaptations. This improves simulation stability during coarse and fine graining by preventing shocks from being generated by the sudden addition or removal of atoms.

The examples presented illustrate the efficiency and energy conservation properties of the method. It is shown that the method provides a significant speedup versus fully MD solutions, while allowing defects to propagate freely without the *a priori* knowledge of the solution other multiscale methods require. The energy conservation is shown to be within acceptable boundaries, and several explanations are given for the energy growth seen.

The techniques and algorithms used in this method allow simulations to combine the advantages of FEM, XFEM, and MD in a way that is flexible and computationally efficient. The method retains the advantages of multiscale simulation, in addition to the freedom of adaptivity. These features enable enhanced research in accurate prediction of material fracture and failure.

ACKNOWLEDGMENT

We gratefully acknowledge grant support from the Office of Naval Research under award N0014-08-1-1191.

REFERENCES

Abraham, F., Broughton, J., Bernstein, N., and Kaxiras, E., Spanning the continuum to quantum length scales in a dynamic simulation of brittle fracture, *Europhys. Letters*, vol. **44**, no. 6, pp. 783–787, 1998.

Areias, P. and Belytschko, T., Two-scale shear band evolution by local partition of unity, *Int. J. Numer. Methods Eng.*, vol. **66**, no. 5, pp. 878–910, 2006.

Bauman, P., Dhia, H., Elkhodja, N., Oden, J., and Prudhomme, S., On the application of the arlequin method to the coupling of particle and continuum models, *Comput. Mech.*, vol. **42**, no. 4, pp. 511–530, 2008.

Belytschko, T. and Black, T., Elastic crack growth in finite elements with minimal remeshing, *Int. J. Numer. Methods Eng.*, vol. **45**, no. 5, pp. 601–620, 1999.

Belytschko, T., Gracie, R., and Ventura, G., A review of extended/generalized finite element methods for material modeling, *Model. Simul. Mater. Sci. Eng.*, vol. **17**, p. 043001, 2009.

Belytschko, T., Parimi, C., Moes, N., Sukumar, N., and Usui, S., Structured extended finite element methods for solids defined by implicit surfaces, *Int. J. Numer. Methods Eng.*, vol. **56**, no. 4, pp. 609–635, 2003.

Belytschko, T. and Xiao, S., Coupling methods for continuum model with molecular model, *Int. J. Multiscale Comput. Eng.*, vol. **1**, no. 1, pp. 115–126, 2003.

Belytschko, T., Xiao, S., Schatz, G., and Ruoff, R., Atomistic simulations of nanotube fracture, *Phys. Rev. B*, vol. **65**, no. 23, p. 235430, 2002.

Ben Dhia, H., Multiscale mechanical problems: the arlequin method, *Comptes Rendus de Academie des Sciences Series IIb*, vol. **326**, pp. 899–904, 1998.

Berendsen, H., Postma, J., Van Gunsteren, W., DiNola, A., and Haak, J., Molecular dynamics with coupling to an external bath, *J. Chem. Phys.*, vol. **81**, p. 3684, 1984.

Broughton, J., Abraham, F., Bernstein, N., and Kaxiras, E., Concurrent coupling of length scales: Methodology and application, *Phys. Rev. B*, vol. **60**, no. 4, pp. 2391–2403, 1999.

Chamoin, L., Prudhomme, S., Ben Dhia, H., and Oden, T., Ghost forces and spurious effects in atomic-to-continuum coupling methods by the arlequin approach, *Int. J. Numer. Methods Eng.*, vol. **83**, nos. 8-9, pp. 1081–1113, 2010.

Chessa, J. and Belytschko, T., An enriched finite element method for two-phase fluids, *ASME J. Appl. Mech.*, vol. **70**, no. 1, pp. 10–17, 2003.

Fish, J., Nuggehally, M., Shephard, M., Picu, C., Badia, S., Parks, M., and Gunzburger, M., Concurrent ATC coupling based on a blend of the continuum stress and the atomistic force, *Comput. Methods Appl. Mech. Eng.*, vol. **196**, nos. 45-48, pp. 4548–4560, 2007.

Girifalco, L. and Weizer, V., Application of the morse potential function to cubic metals, *Phys. Rev.*, vol. **114**, no. 3, p. 687, 1959.

Gracie, R. and Belytschko, T., Concurrently coupled atomistic and xfem models for dislocations and cracks, *Int. J. Numer. Methods Eng.*, vol. **78**, no. 3, pp. 354–378, 2008.

Gracie, R. and Belytschko, T., An adaptive concurrent multiscale method for the dynamic simulation of dislocations, *Int. J. Numer. Methods Eng.*, vol. **86**, nos. 4-5, pp. 575–597, 2011.

Gracie, R., Oswald, J., and Belytschko, T., On a new extended finite element method for dislocations: Core enrichment and nonlinear formulation, *J. Mech. Phys. Solids*, vol. **56**, no. 1, pp. 200–214, 2008.

Miller, R. and Tadmor, E., The quasicontinuum method: Overview, applications and current directions, *J. Comput.-Aided Mater. Des.*, vol. **9**, no. 3, pp. 203–239, 2002.

Miller, R. and Tadmor, E., A unified framework and performance benchmark of fourteen multiscale atomistic/continuum coupling methods, *Model. Simul. Mater. Sci. Eng.*, vol. **17**, p. 053001, 2009.

Moës, N., Dolbow, J., and Belytschko, T., A finite element method for crack growth without remeshing, *Int. J. Numer. Methods Eng.*, vol. **46**, no. 1, pp. 131–150, 1999.

Moseley, P., Oswald, J., and Belytschko, T., Adaptive atomistic-to-continuum modeling of propagating defects, *Int. J. Numer. Methods Eng.*, vol. **92**, no. 10, pp. 835–856, 2012.

Mullins, M. and Dokainish, M., Simulation of the (001) plane crack in α-iron employing a new boundary scheme, *Philos. Mag. A*, vol. **46**, no. 5, pp. 771–787, 1982.

Oswald, J., Gracie, R., Khare, R., and Belytschko, T., An extended finite element method for dislocations in complex geometries: Thin films and nanotubes, *Comput. Methods Appl. Mech. Eng.*, vol. **198**, nos. 21-26, pp. 1872–1886, 2009.

Qu, S., Shastry, V., Curtin, W., and Miller, R., A finite-temperature dynamic coupled atomistic/discrete dislocation method, *Model. Simul. Mater. Sci. Eng.*, vol. **13**, p. 1101, 2005.

Shenoy, V. B., Miller, R., Tadmor, E. B., Phillips, R., and Ortiz, M., Quasicontinuum models of interfacial structure and deformation, *Phys. Rev. Lett.*, vol. **80**, no. 4, pp. 742–745, 1998.

Shilkrot, L. E., Miller, R. E., and Curtin, W. A., Multiscale plasticity modeling: Coupled atomistics and discrete dislocation mechanics, *J. Mech. Phys. Solids*, vol. **52**, no. 4, pp. 755–787, 2004.

Tadmor, E., Ortiz, M., and Philips, R., Quasicontinuum analysis of defects in solids, *Philos. Mag. A*, vol. **73**, no. 6, pp. 1529–1563, 1996.

Ventura, G., Gracie, R., and Belytschko, T., Fast integration and weight function blending in the extended finite element method, *Int. J. Numer. Methods Eng.*, vol. **77**, no. 1, pp. 1–29, 2009.

Xiao, S. and Belytschko, T., A bridging domain method for coupling continua with molecular dynamics, *Comput. Methods Appl. Mech. Eng.*, vol. **193**, pp. 1645–1669, 2004.

Xu, M. and Belytschko, T., Conservation properties of the bridging domain method for coupled molecular/continuum dynamics, *Int. J. Numer. Methods Eng.*, vol. **76**, pp. 278–294, 2008.

Xu, M., Gracie, R., and Belytschko, T., A continuum-to-atomistic bridging domain method for composite lattices, *Int. J. Numer. Methods Eng.*, vol. **81**, no. 13, pp. 1635–1658, 2010.